



Green assembly of stable and uniform silver nanoparticles on 2D silica nanosheets for catalytic reduction of 4-nitrophenol



Zhaoli Yan^{a,b}, Liangjie Fu^{a,b}, Xiaochao Zuo^{a,b}, Huaming Yang^{a,b,c,*}

^a Centre for Mineral Materials, School of Minerals Processing and Bioengineering, Central South University, Changsha 410083, China

^b Hunan Key Lab of Mineral Materials and Application, Central South University, Changsha 410083, China

^c State Key Lab of Powder Metallurgy, Central South University, Changsha 410083, China

ARTICLE INFO

Keywords:

Kaolinite
2D silica nanosheets
Silver nanoparticles
Modified in-situ reduction approach
Catalytic reduction

ABSTRACT

A facile, environment-friendly route is illustrated for the efficient assembly of stable and uniform silver nanoparticles (AgNPs) on the surface of two-dimensional (2D) silica nanosheets (SiNSs, derived from natural kaolinite mineral) via in-situ reduction using Sn(II) as reductant. Compared to the common reduction method using NaBH₄ reductant, the loaded AgNPs on AgNPs/SiNSs nanocomposite showed higher purity, uniformity and stability (antioxygenation). The catalytic reduction of 4-nitrophenol (4-NP) over AgNPs/SiNSs nanocatalyst was almost complete within 40 s without stirring and the apparent kinetic rate constant k_{app} ($80.19 \times 10^{-3} \text{ s}^{-1}$) is much higher than those of other substrate-supported Ag/Au nanocatalysts. The effects of support material and assembly approach of AgNPs on the catalytic performance were discussed in detail. The high turnover frequency (TOF) for AgNPs/SiNSs nanocatalyst (3.52 min^{-1}) indicates that the high-density dispersion of uniform small-sized AgNPs on 2D SiNSs surface is responsible for the excellent catalytic property, which offer many active sites for effective contact with the reactants and fast interfacial electron transfer from the AgNPs surface to 4-NP. It exhibits the great potential of 2D silica nanosheets as support materials for the efficient assembly of uniform noble-metal nanoparticles. Moreover, the 2D AgNPs/SiNSs nanocomposite holds a stable catalytic efficiency (around 100%) over five reaction cycles. The high efficiency and convenience have been demonstrated by purifying the 4-NP polluted water in the “filtering and catalyzing” device, in which the polluted water could become colorless within 10 s.

1. Introduction

Noble metals, especially gold and silver nanoparticles (NPs), have become significant in many fields, including catalysis, photochemistry, optoelectronics, energy conversion, and biomedicine [1–6]. Although silver is relatively more abundant and lower in cost, gold NPs are widely favoured because they are highly stable and easy to use. Contrarily, silver NPs are famously susceptible to oxidation, which has seriously limited the development and application of silver-based nanomaterials [7–11]. The noble-metal NPs are usually assembled on the surface of solid substrates (e.g., metal oxides, zeolites, clays, carbons, and organic polymers) for facile recovery and recycling [12]. However, the reductants used for the chemical reduction of noble-metal ions are usually hydrazine or sodium borohydride (NaBH₄), which shows highly toxic. [13] Thus, a facile, environmentally friendly approach for the effectively assembly of noble-metal NPs needs to be explored. Between 2007 and 2012, an in-situ reduction approach using Sn(II) as reductant was developed to deposit highly dispersed noble-metal NPs onto the

surface of hydroxyl-group-rich supports (e.g., silica nanotubes and titania precursors), unfortunately, the utilisation rate of noble-metal precursors in this method was low and the content of noble-metal NPs on these substrates was difficult to control [14–16]. For example, Zhang et al. assembled silver nanoparticles (AgNPs) on electrospun silica nanotubes by this method, but with a decrease in the mean particle diameter from 7.68 to 2.85 nm, the loading of AgNPs was decreased from 11.20 to 5.40 wt.%, while the calculated theoretical AgNPs content approaches 35 wt.% [16]. It seriously limited the application of the in-situ reduction approach using Sn(II) as reductant, and for which the relevant study is rare now. Hence, a modified in-situ reduction route and suitable support materials must be developed for the efficient assembly of uniform noble-metal NPs. What's more, a lot of questions arise about this in-situ reduction approach, such as the effect of the Sn (II) reductant on the growth process of noble-metal NPs, the influence of the remained Sn(II) species in the nanocomposites on the stability of noble-metal NPs (especially AgNPs), and the difference between the in-situ reduction approach and the common reduction method using

* Corresponding author at: Centre for Mineral Materials, School of Minerals Processing and Bioengineering, Central South University, Changsha, 410083, China.
E-mail address: hmyang@csu.edu.cn (H. Yang).

NaBH_4 reductant.

4-nitrophenol (4-NP) is one of the most commonly used organic pollutants in the production of pesticides and dyes, and is genotoxic and carcinogenic to human and animals [17,18]. And, 4-aminophenol (4-AP) is an important industrial intermediate applied in various fields including corrosion inhibition, analgesic and antipyretic drugs, and photographic developers [19,20]. The reduction of 4-NP over noble-metal NPs in the presence of NaBH_4 is an efficient and eco-friendly route to produce 4-AP [21–24]. Thus, the reduction of 4-NP to 4-AP with excessive NaBH_4 was selected as a model reaction to quantitatively evaluate the catalytic properties.

In this work, the efficient assembly and high-density dispersion of uniform AgNPs was achieved on the surface of two-dimensional (2D) silica nanosheets (SiNSs, derived from natural kaolinite mineral) by a green in-situ reduction approach using Sn(II) as reductant. In particular, this modified in-situ reduction approach caused the initial synthesis of silver nanoclusters (AgNCs, < 2 nm) on the surface of 2D-SiNSs during the in-situ reduction reaction, which then grow into small AgNPs (~ 2.77 nm) in the washing process due to the absence of ammonia solution, and the loaded AgNPs have higher purity compared to that by common reduction method using NaBH_4 . The stability (anti-oxygenation) of AgNPs in AgNPs/SiNSs nanocomposite and the effect of the Sn(II) species remaining in the AgNPs/SiNSs were demonstrated by comparing with the common reduction method. The as-prepared AgNPs/SiNSs nanocatalyst possessed excellent catalytic property for the reduction of 4-NP by NaBH_4 , and the effects of support material and assembly approach of AgNPs on the catalytic performance were discussed in detail.

2. Experimental

2.1. Material preparation

Natural kaolinite was obtained from China Kaolin Clay Co., Ltd (Suzhou, China). The major components (wt.%) were SiO_2 53.27%, Al_2O_3 42.46%, Fe_2O_3 0.48%, TiO_2 0.33%, K_2O 0.54%, CaO 0.09%, MgO 0.16%, P_2O_5 0.26%, and SO_3 2.19%.

In a typical preparation of the silica nanosheets, kaolinite was first converted to anhydrous metakaolinite by calcining at 700 °C for 2 h. Then, 2 g of metakaolinite was treated with 100 mL of 2 M HCl solution at 85 °C for 8 h. The resulting precipitate was filtered, repeatedly washed with deionised water, dried at 110 °C for 12 h, and ground into fine powder. The resultant product was silica nanosheets, denoted as SiNSs.

1 g of SiNSs was fully dispersed in 100 mL deionised water, 0.15 g of $\text{SnCl}_2 \cdot 2\text{H}_2\text{O}$ was dissolved in 30 mL of 0.01 M HCl solution, and then the above solution was reacted under vigorous stirring for 8 h at room temperature. After this, the precipitate was recovered by centrifugation, followed by washing four times with deionised water. Thus, the Sn^{2+} -activated SiNSs (Sn^{2+} -SiNSs) were obtained. Afterward, 0.2 g of as-prepared Sn^{2+} -SiNSs was fully dispersed in 30 mL of deionised water, to which 1.5 mL of ammonia solution was added, followed by adding 20 mL of 3 mM AgNO_3 solution gradually under vigorous stirring. This mixture was stirred constantly for 2 h. The resultant precipitate was filtered, repeatedly washed with deionised water, dried for 6 h at 60 °C under vacuum, and ground into fine powders. The resulting product was Ag nanoparticles/silica nanosheets (AgNPs/SiNSs). For comparison, AgNPs were also assembled on SiNSs by the common reduction method using NaBH_4 reductant. 0.2 g SiNSs was dispersed in 30 mL deionised water under ultrasonication for 10 min, followed by adding 20 mL of 3 mM AgNO_3 solution, and then 10 mL deionised water containing 3 mg NaBH_4 was added dropwise under stirring for 30 min. The resultant precipitate was filtered, repeatedly washed with deionised water, dried for 6 h at 60 °C under vacuum, ground into fine powder, and denoted as AgNPs/SiNSs-1.

2.2. Characterization

The compositions of the samples were determined by a PANalytical Axios mAX wavelength dispersive X-ray fluorescence (XRF) spectrometer. Scanning electron microscopy (SEM) combined with energy-dispersive X-ray spectroscopy (EDS) analysis was conducted on a Tescan Mira3 LMU. N_2 adsorption measurements were performed at 77 K using a Micromeritics ASAP 2020 gas sorption instrument. Before measurements, the samples were degassed at 120 °C for more than 6 h. The specific surface areas were calculated using the multi-point Brunauer–Emmett–Teller (BET) method, and the total pore volumes (V_{tot}) were estimated from the adsorbed volumes at a relative pressure (P/P_0) of 0.995. Scanning transmission electron microscopy (STEM) combined with EDS analysis was performed using a Titan G2 60-300 microscope operating at an accelerating voltage of 300 kV. Samples were dispersed in ethanol by ultrasound for 20 min, and then deposited on holey carbon-coated copper grids. X-ray photoelectron spectroscopy (XPS) analysis was performed on a Thermo Scientific Escalab 250Xi spectrometer equipped with an Al $K\alpha$ monochromated X-ray source. The binding energy (BE) was referenced to the C 1 s peak at 284.6 eV. UV-vis absorption spectra were measured at room temperature with a Shimadzu UV-2600 UV-vis spectrophotometer.

2.3. Catalytic reduction of 4-nitrophenol (4-NP)

10 mg of the as-prepared samples (Sn^{2+} -SiNSs, AgNPs/SiNSs and AgNPs/SiNSs-1) were fully dispersed in 50 mL of 0.12 mM 4-NP solution. Subsequently, 3.0 mL of the above solution was transferred into a quartz cuvette, and fresh NaBH_4 solution (0.2 mL, 0.3 M) was added. The absorbance changes of the 4-NP ions were monitored at $\lambda_{max} = 400$ nm using a UV-vis spectrophotometer after appropriate time intervals. To investigate the reusability of the AgNPs/SiNSs catalyst, 20 mg of the sample and the corresponding amounts of 4-NP and fresh NaBH_4 solutions noted previously were used. The reaction was performed at room temperature for 1 min with continuous stirring, and then 3 mL of the mixture was filtered through a 0.22- μm membrane filter, and measured by UV-vis spectrophotometer. The catalyst was separated and reused for 5 cycles under the same reaction procedure.

3. Results and discussion

3.1. Catalyst preparation and characterization

The schematic of the preparation of AgNPs/SiNSs is displayed in Fig. 1. First, based on the features of layered clay minerals [25–34], SiNSs ($\text{Si}_2\text{O}_3(\text{OH})_2$) are obtained from natural kaolinite ($\text{Al}_1\text{Si}_2\text{O}_5(\text{OH})_4$) through a thermal activation and Al-leaching treatment [35–37]. Unlike the framework structure of general silica gels, most of the hydroxyl groups here are associated with a silanol group represented by the $\text{Si}(\text{OSi})_3\text{OH}$ unit (Q^3) on one side of the SiNSs [37,38]. The corresponding SEM images of kaolinite and SiNSs show preservation of a sheet-like morphology (200–500 nm) and the exfoliated dispersion of original kaolinite layer structure (Fig. S1a and b), as confirmed by the significant increase in specific surface area from 20 to $312 \text{ m}^2 \text{ g}^{-1}$ (Table S1). Compared to the reported 0D silica nanoparticles and 1D silica nanotubes [15,16], 2D SiNSs may provide more accessible hydroxyl groups to link with more Sn(II) ions, further ensuring the full loading and high dispersion of uniform AgNPs through the in-situ reduction approach. Actually, Sn(II) species exhibit strong reducibility in weak acid solution. In order to inhibit the reducibility of Sn(II) species, further preventing the silver nanostructures growth during the in-situ reduction reaction, ammonia solution (or dilute sodium hydroxide solution) should be added before the silver precursors to create alkaline conditions. Therefore, AgNCs were likely to be first formed on the surface of 2D-SiNSs during the in-situ reduction reaction, and then further grew into small AgNPs in the subsequent washing

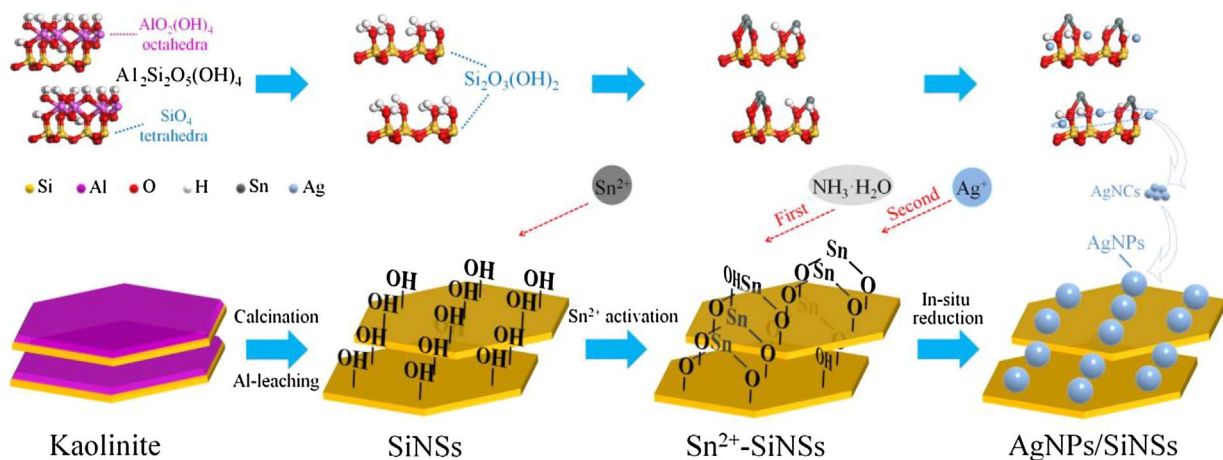


Fig. 1. Schematic for the preparation of AgNPs/SiNSs.

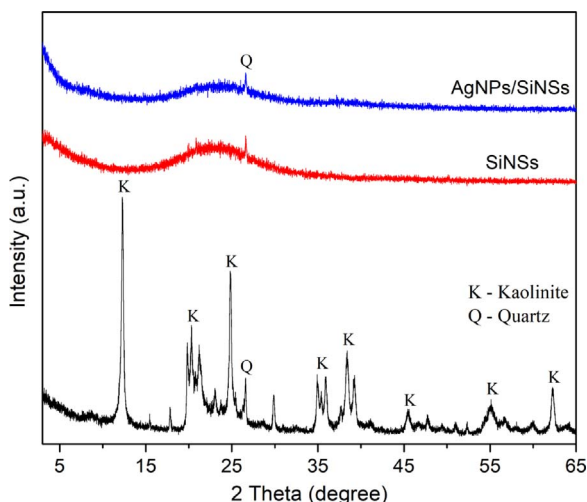


Fig. 2. XRD patterns of kaolinite, SiNSs and AgNPs/SiNSs samples.

process due to the enhanced reducibility of Sn(II) species in the absence of ammonia solution.

From the XRD patterns (Fig. 2), the as-received kaolinite corresponds to kaolinite-1A ($\text{Al}_2\text{Si}_2\text{O}_5(\text{OH})_4$, JCPDS 14-0164) containing trace quartz impurities [35]. After modification, the obtained SiNSs exhibit a broad diffraction peak centred at $2\theta \approx 23^\circ$, attributed to amorphous silica. The XRD pattern of AgNPs/SiNSs is similar to that of SiNSs, without the diffraction reflections ascribed to AgNPs, perhaps because of the low content and/or very small size of AgNPs. However, after AgNPs loading, the intensity of the diffraction peak attributed to silica is obviously decreased.

Transmission electron microscopy (TEM) and high-resolution TEM (HRTEM) images of AgNPs/SiNSs clearly show the successful loading of AgNPs (< 5 nm) on the surfaces of the 2D-SiNSs (Fig. 3a and b). The energy-dispersive X-ray spectroscopy (EDS) data also proves the presence of Si (44.05 wt.%), O (45.52 wt.%), Al (0.75 wt.%), Sn (6.92 wt.-%), and Ag (2.76 wt.-%) (inset of Fig. 3a). The loading amount of AgNPs is near the theoretical value of 3.00 wt.-%, which is also near the 3.26 wt.% value determined by XPS analysis (Table S2). In addition, the SAED pattern of AgNPs/SiNSs shows an amorphous framework from the very small AgNPs (Fig. 3c), which is consistent with the XRD patterns of AgNPs/SiNSs (Fig. 2). To visually observe the dispersion and size distribution of AgNPs, a high angle annular dark field-scanning TEM (HAADF-STEM) image and size distribution histogram of the AgNPs (inset) are displayed in Fig. 3d. These indicate a high-density dispersion of AgNPs with a narrow size distribution from 1.6 to 4 nm

(mean size = 2.77 nm). The corresponding quantitative EDS maps also illustrate the homogeneous distribution of Sn and Ag on the surface of AgNPs/SiNSs (Fig. 3e–g). Compared with the previous in-situ reduction method [36], the modified in-situ reduction approach in this work can achieve more uniform and smaller AgNPs, according to the STEM images (Fig. S1c and d).

Further investigation on the synthesis process of AgNPs on the SiNSs surface via in-situ reduction approach were performed by the ultra-violet-visible (UV-vis) absorption spectra of the aqueous suspension in the preparation process (Fig. 4(a–d)). The UV-vis absorption spectrum for the aqueous suspension of AgNPs/SiNSs-1 sample (prepared by the common reduction method using NaBH_4) is also provided for the comparison with that of AgNPs/SiNSs sample (Fig. 4e and d). No distinct adsorption peaks appear for the aqueous suspension of Sn^{2+} -SiNSs in the visible region (Fig. 4a), while AgNPs/SiNSs under different washing degrees in the preparation process (Fig. 4(b–d)) exhibit some broad surface plasmon resonance peaks (SPRPs) [23,39–42]. For the unwashed AgNPs/SiNSs (U-AgNPs/SiNSs) in Fig. 4b, the SPRPs at approximately 360 and 412 nm are the widest, indicating that the silver nanostructures this moment in the preparation process are the smallest. With the increase of washing cycles, the silver nanostructures gradually grow, causing the SPRPs to narrow and increase in intensity [43], and introducing new SPRPs at longer wavelengths (at 465 nm for W-AgNPs/SiNSs and 483 nm for AgNPs/SiNSs). Correspondingly, the aqueous suspension of Sn^{2+} -SiNSs is white color because of the absence of absorption peaks in the visible spectrum (insert of Fig. 4), while that of AgNPs/SiNSs under different washing degrees are lightyellow, yellow-orange, and red-brown in accordance with the increased sizes of the silver nanostructures. Considering that the mean AgNPs size in AgNPs/SiNSs nanocomposite is 2.77 nm (Fig. 3d), we have reason to believe that the size of the silver nanostructures in U-AgNPs/SiNSs during the preparation process is mainly below 2 nm, on the scale of AgNCs. It indicates that for in-situ reduction approach, AgNCs of < 2 nm were first synthesised on the SiNSs surface during the in-situ reduction reaction and subsequently grow into small AgNPs during washing, which confirmed the synthesis process (Fig. 1). Moreover, for the common reduction method, the UV-vis absorption spectrum shows a very broad SPRP at 498 nm (Fig. 4e), indicating the larger AgNPs with a broad size distribution on the AgNPs/SiNSs-1 surface than those on AgNPs/SiNSs surface. And the existence of an obvious absorption peak at 300 nm characteristic of silver ion (Ag^+) indicates that the AgNPs on AgNPs/SiNSs-1 surface are not pure enough. Therefore, the loaded AgNPs on SiNSs surface via in-situ reduction approach have higher uniformity (consistent with the STEM observation in Fig. 3d), and greater purity than that via the common reduction method using NaBH_4 reductant.

To clarify the advantage of AgNPs/SiNSs nanocomposite prepared by in-situ reduction approach in this work, the XPS survey spectra and

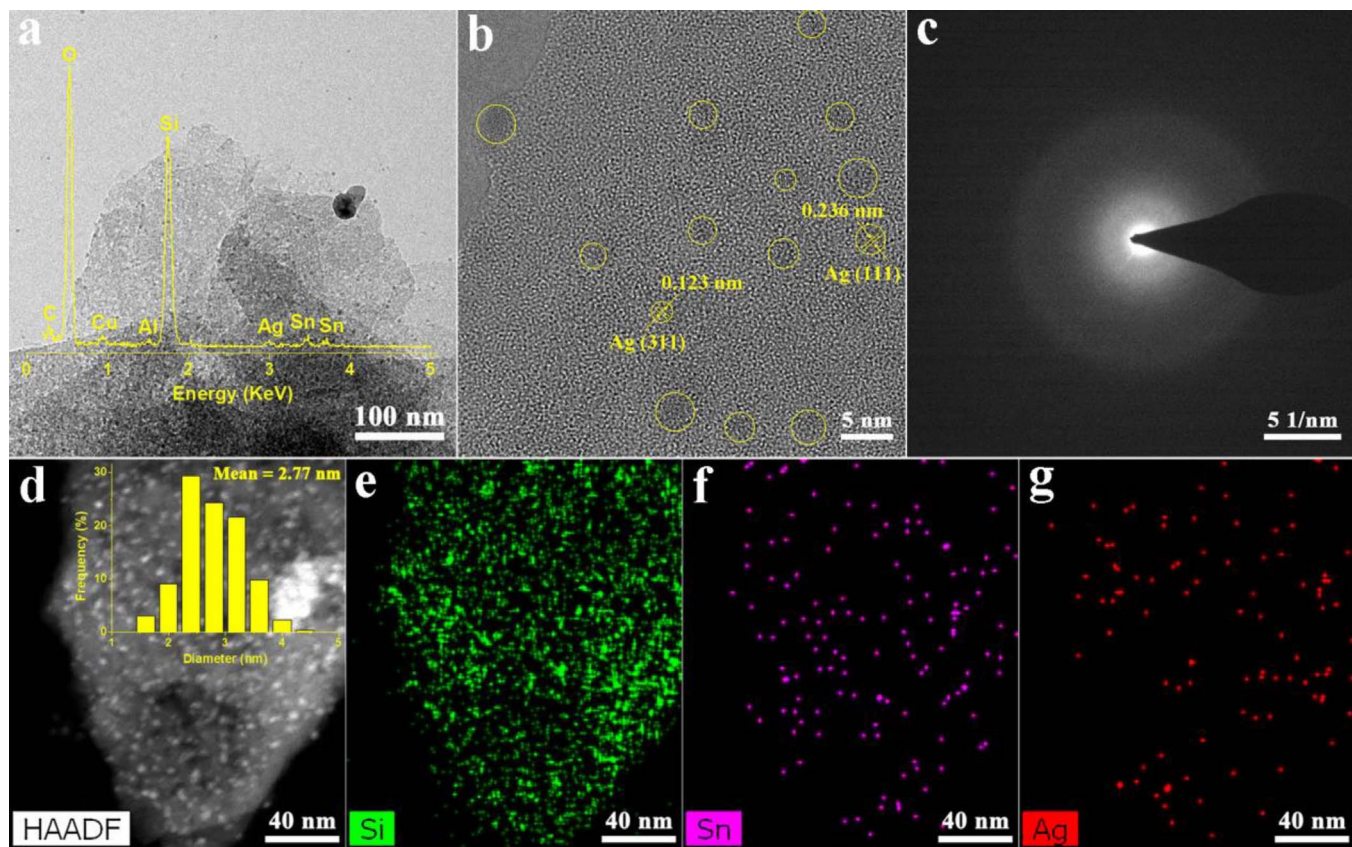


Fig. 3. (a) TEM image (inserted EDS spectrum), (b) HRTEM image, (c) SAED pattern, (d) HAADF-STEM image (inserted the size distribution histogram of AgNPs); corresponding quantitative EDS maps for (e) Si, (f) Sn, (g) Ag elements of AgNPs/SiNSs.

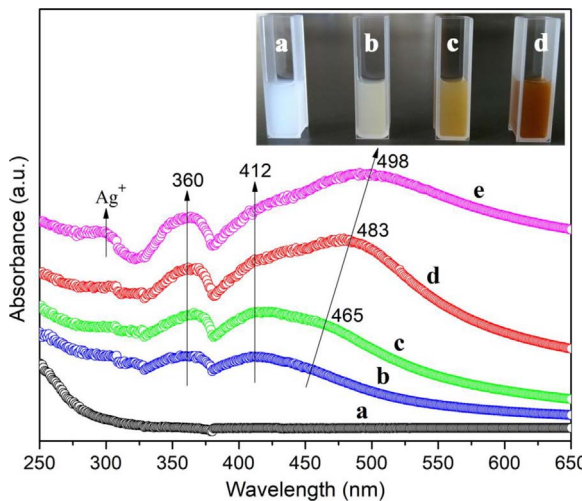


Fig. 4. UV-vis absorption spectra of aqueous suspensions (inset: digital photographs) of (a) Sn^{2+} -SiNSs; AgNPs/SiNSs under different washing degrees in the preparation process; (b) U-AgNPs/SiNSs (unwashed), (c) W-AgNPs/SiNSs (washed one time) and (d) AgNPs/SiNSs (fully washed); (e) AgNPs/SiNSs-1 sample. Baseline is from the aqueous suspension of SiNSs.

high-resolution XPS spectra of AgNPs/SiNSs and AgNPs/SiNSs-1 are displayed (Fig. 5), and the survey spectra show the existence of Si, O, Sn, and Ag in AgNPs/SiNSs, and the existence of Si, O, and Ag elements in AgNPs/SiNSs-1 (Fig. 5a). The presence of C is attributed to surface-absorbed carbon-based contaminant. Subsequently, the O 1s high-resolution XPS spectra are analyzed (Fig. 5b). The binding energies at approximately 533.7 eV and 532.8 eV are attributed to the surface hydroxyl groups of silica ($\text{Si}-\text{O}-\text{H}$) and the crystal lattice oxygen of silica

($\text{Si}-\text{O}-\text{Si}$), respectively. In addition, for AgNPs/SiNSs-1, the peak at 532.0 eV is ascribed to the formation of a $\text{Si}-\text{O}-\text{Ag}$ unit on the surfaces of SiNSs. For AgNPs/SiNSs, the peak with a lower binding energy at 531.8 eV is assigned to $\text{Si}-\text{O}-\text{Ag}(\text{Sn})$, suggesting the formation of $\text{Si}-\text{O}-\text{Ag}$ units through the reduction of Ag^+ by Sn^{2+} on the surface of SiNSs. Furthermore, the Sn 3d spectrum of AgNPs/SiNSs is displayed (Fig. 5c). According to the literature and our previous work [16,36], the peak position for $\text{Sn } 3d_{5/2}$ at 487.3 eV coincides with the assignment for Sn^{2+} , although some Sn^{4+} ions may be adsorbed on the surface of the SiNSs by the reduction of Ag^+ by Sn^{2+} . The Ag 3d spectra of AgNPs/SiNSs and AgNPs/SiNSs-1 are fitted with two components for the Ag^0 and $\text{Ag}\cdots\text{O}^-$ peaks (Fig. 5d). The Ag species in the $\text{Ag}\cdots\text{O}^-$ peaks should be Ag^0 and/or Ag^+ attached to O species. In the spectra of AgNPs/SiNSs, the splittings of the Ag 3d doublet for Ag^0 and $\text{Ag}\cdots\text{O}^-$ peaks are all approximately 6 eV, demonstrating that Ag exists as Ag^0 in AgNPs/SiNSs. However, in the spectrum of AgNPs/SiNSs-1, only the splitting of the Ag 3d doublet for Ag^0 peaks is around 6 eV, while that for $\text{Ag}\cdots\text{O}^-$ peaks is 5.85 eV, showing the existence of Ag^+ in AgNPs/SiNSs-1. This indicates that the modified in-situ reduction approach in this work can obtain AgNPs of greater purity than those yielded by the common reduction method using NaBH_4 , consistent with the UV-vis absorption spectra results (Fig. 4).

To determine the effect of Sn(II) species remaining in the AgNPs/SiNSs on the AgNPs stability, the AgNPs/SiNSs and AgNPs/SiNSs-1 samples were treated by oxidation in air at 40 °C for 168 h. From the XPS spectra (Fig. 6), the binding energies of Ag 3d for AgNPs/SiNSs do not change after oxidation treatment, while the binding energy of $\text{Sn } 3d_{5/2}$ shifts by 0.12 eV to a lower binding energy, suggesting that the oxidized Ag may be further reduced by the linked Sn(II) species on the surface of AgNPs/SiNSs. Meanwhile, after oxidation treatment, shifts of 0.16 and 0.30 eV to higher binding energies are observed in AgNPs/SiNSs-1 for the peaks attributed to Ag^0 and

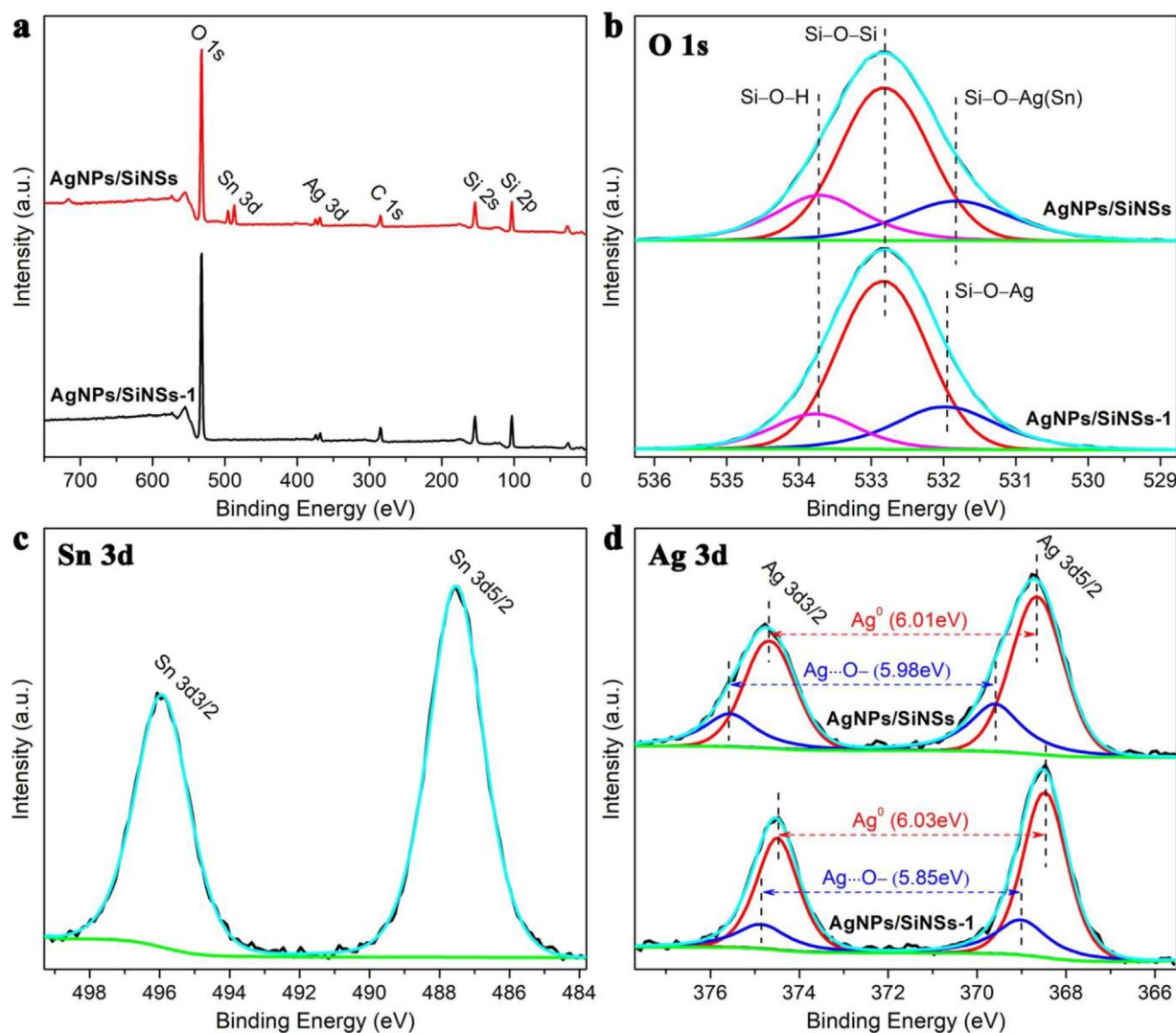


Fig. 5. (a) XPS survey spectra and High-resolution (b) O 1s, (c) Sn 3d, (d) Ag 3d spectra of AgNPs/SiNSs and AgNPs/SiNSs-1.

$\text{Ag}\cdots\text{O}^-$, respectively. The Ag species in $\text{Ag}\cdots\text{O}^-$ peaks should be Ag^0 and/or Ag^+ attached to the O species (Fig. 5). The greater shift (0.30 eV) of the peak attributed to $\text{Ag}\cdots\text{O}^-$ may be related to the

increase of Ag^+ after oxidation treatment. In conclusion, the existence of Sn(II) species stabilises the AgNPs in AgNPs/SiNSs nanocomposite, making them less oxidative.

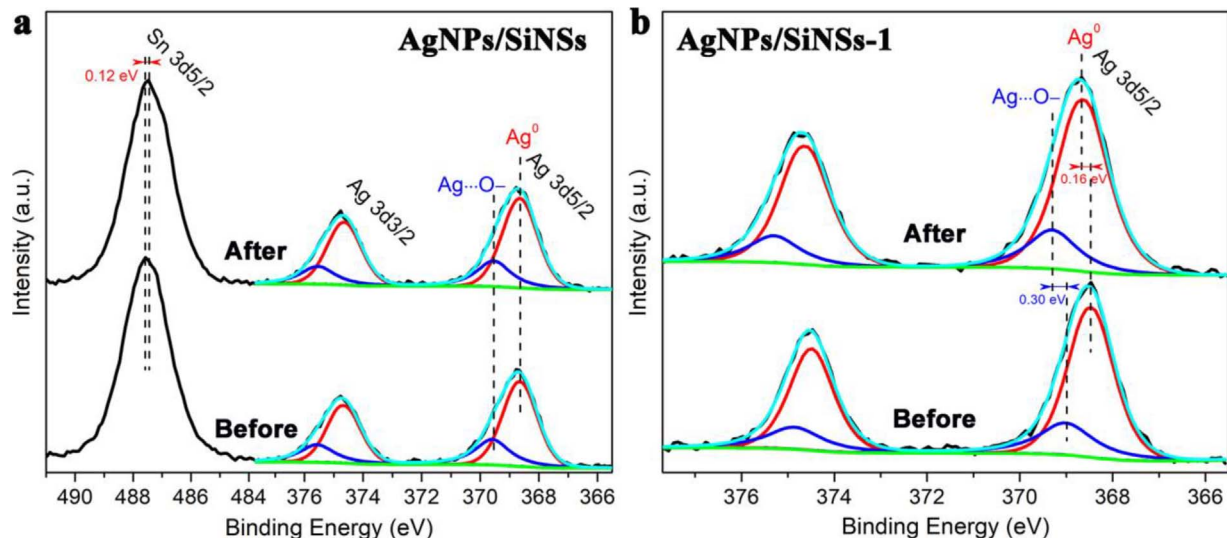


Fig. 6. The Sn 3d and Ag 3d XPS spectra of (a) AgNPs/SiNSs and (b) AgNPs/SiNSs-1 samples before and after oxidation treatment in air at 40 °C for 168 h.

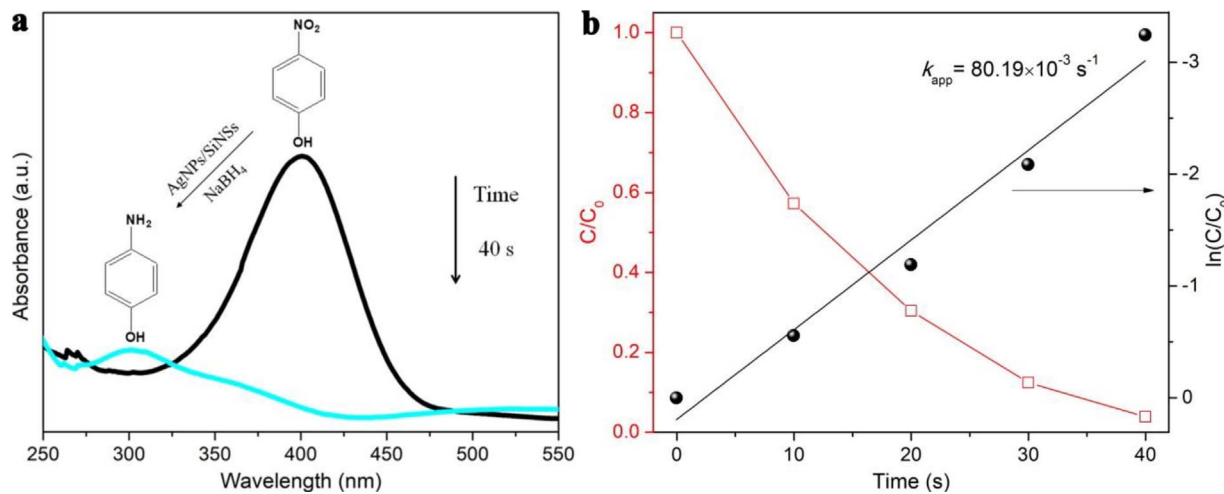


Fig. 7. (a) UV-vis absorption spectra during the catalytic reduction of 4-NP over AgNPs/SiNSs nanocomposite, here baseline is from the aqueous suspension of AgNPs/SiNSs (0.2 g/L); (b) the C/C_0 and $\ln(C/C_0)$ versus reaction time for the catalytic reduction of 4-NP over AgNPs/SiNSs nanocomposite in the presence of NaBH_4 .

3.2. Catalyst activity

The reduction of 4-NP to 4-AP was selected as a model for testing the catalytic activity of AgNPs/SiNSs nanocomposite, and the reaction was determined by UV-vis spectroscopy. As is known, the reduction of 4-NP by NaBH_4 is feasible thermodynamically because the difference of their standard electrode potentials ($\Delta E^0 = E_{(\text{4-NP}/\text{4-AP})}^0 - E_{(\text{CH}_3\text{BO}_3/\text{BH}_4)}^0 = -0.76 - (-1.33) = 0.57 \text{ V}$) is greater than zero, but it could be kinetically restricted in the absence of an efficient catalyst [44]. It is also noted that the 4-NP solution changes from light yellow to bright yellow after adding NaBH_4 , which is caused by the formation of 4-nitrophenolate ions under basic conditions. And the absorption peak of 4-NP solution also shifts from 317 nm to 400 nm [13,16,45].

A controlled experiment was first performed for comparison, and the catalytic performance of Sn^{2+} -SiNSs for the reduction of 4-NP was displayed in Fig. S2. As Sn^{2+} -SiNSs is added into the reaction solution, the concentration of 4-NP is almost unchanged, indicating that the Sn (II) species have no effect on the catalytic reaction. It also excludes the influence of adsorption caused by 2D SiNSs. Fig. 7a shows the UV-vis absorption spectra during the catalytic reduction of 4-NP over AgNPs/SiNSs nanocomposite. In the presence of NaBH_4 , the 4-NP solution exhibits a strong absorption peak at 400 nm. This characteristic absorption peak of 4-NP ions disappears in 40 s after the addition of the AgNPs/SiNSs catalyst, while a new peak ascribed to 4-AP appears at approximately 300 nm. Fig. 7b further indicates the excellent catalytic property of the AgNPs/SiNSs nanocomposite. The catalytic reaction is almost complete within 40 s without stirring. The apparent kinetic rate constant k_{app} can be defined as $dC/dt = k_{\text{app}}C$, where C is the concentration of 4-NP at reaction time t . It is well known this reaction follows pseudo-first order kinetics towards the concentration of 4-NP in the presence of excess NaBH_4 . Here a linear correlation is found between $\ln(C/C_0)$ and the reaction time, confirming pseudo-first order kinetics, and the corresponding value of k_{app} can be calculated from the slope as approximately $80.19 \times 10^{-3} \text{ s}^{-1}$ for the AgNPs/SiNSs nanocomposite, much higher than those of other supported Ag/Au nanocatalysts (Table 1). While for AgNPs/SiNSs-1 sample (Fig. 8), the reaction is almost complete within 180 s without stirring, and k_{app} value is $18.05 \times 10^{-3} \text{ s}^{-1}$. It indicates the higher catalytic performance of AgNPs/SiNSs prepared by in-situ reduction approach than that of AgNPs/SiNSs-1 prepared via the common reduction method.

The turnover frequency (TOF) is one important indicator to access the catalytic activity of noble-metal NPs, which is obtained by dividing the molar mass of the raw 4-NP with the molar mass of the loaded noble-metal NPs and reaction time (Table 1). According to the literatures [16,46,47], the size effect of AgNPs takes a leading role in

Table 1

Comparison of the catalytic performances of various supported Ag/Au nanocatalysts.

Catalyst	Complete reaction time (s)	$k_{\text{app}}^{\text{a}}$ (10^{-3} s^{-1})	TOF ^b (min^{-1})
Ag-NP/C [21]	1500	1.69	0.01
Au-PDA/RGO [13]	960	2.00	0.70
Au/graphene hydrogel [48]	720	3.17	0.55
CNFs/AgNPs [49]	480	6.20	–
AuNPs/SNTs [15]	280	10.64	–
AgNPs/SNTs [16]	90	38.41	0.80
AgNPs/SiNSs	40	80.19	3.52
AgNPs/SiNSs-1	180	18.05	0.80

^a k_{app} : apparent rate constant.

^b TOF: the turnover frequency, the moles of 4-NP reduced per mole of Ag (or Au) per minute.

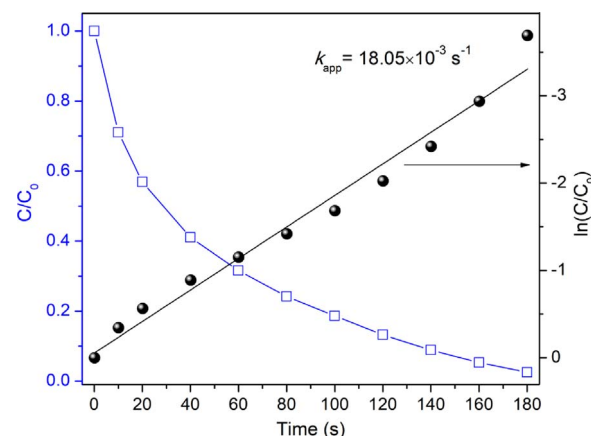


Fig. 8. The C/C_0 and $\ln(C/C_0)$ versus reaction time for the catalytic reduction of 4-NP over AgNPs/SiNSs-1 sample in the presence of NaBH_4 .

improving the catalytic activity due to their size-dependent redox potential and surface-to-volume ratio, which could promote the interfacial electron transfer from the AgNPs surface to 4-NP in the presence of highly electron injecting BH_4^- ions. It well explains the much higher TOF value of AgNPs/SiNSs (3.52 min^{-1}) than that of AgNPs/SiNSs-1 (0.80 min^{-1}) because of the smaller AgNPs on the AgNPs/SiNSs surface than those on AgNPs/SiNSs-1 surface (see Fig. 4d and e), demonstrating faster interfacial electron transfer from the AgNPs surface to 4-NP. Among the other supported Ag nanocatalysts (Table 1), the AgNPs/

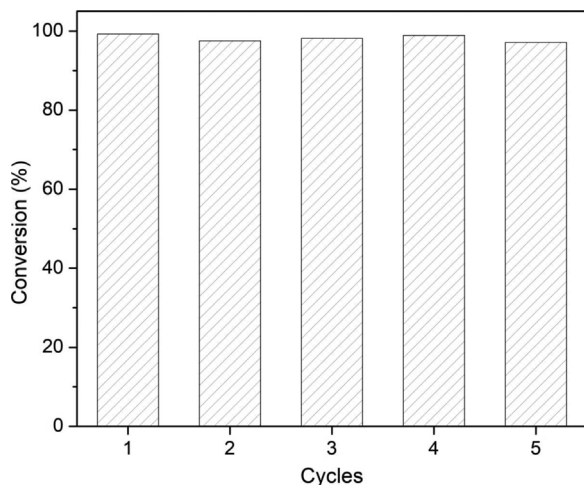


Fig. 9. The reusability of AgNPs/SiNSs catalyst for the reduction of 4-NP with NaBH_4 .

SNTs (silver nanoparticles/silica nanotubes) nanocomposite is a representative comparison due to the similar compositions and the same catalytic reaction conditions with AgNPs/SiNSs ($C_{4\text{-NP}} = 0.12 \text{ mM}$, $C_{\text{catalyst}} = 0.2 \text{ g/L}$) [16]. Obviously, the TOF value of AgNPs/SiNSs is as high as almost 5 times of that for the AgNPs/SNTs catalyst, indicating the higher catalytic activity of AgNPs on the 2D SiNSs surface than that on 1D SNTs surface. Considering the mean-particle-sizes and contents of AgNPs on SiNSs (2.77 nm, 2.76 wt.%) and SNTs (2.85 nm, 5.40 wt.%) surface, the excellent catalytic property of AgNPs/SiNSs nanocomposite is attributed to the high-density dispersion of small-sized AgNPs on the 2D SiNSs surface, offering many active sites for effective contact with the reactants and fast interfacial electron transfer from the AgNPs surface to 4-NP. These results clearly indicate that SiNSs are good support materials for AgNPs because they have high specific surface areas, abundant accessible hydroxyl groups, chemical stability, and 2D nanostructured properties.

Moreover, the reusability of the AgNPs/SiNSs catalyst for the reduction of 4-NP with NaBH_4 is shown in Fig. 9. After five cycles, the high catalytic activity of AgNPs/SiNSs is unchanged. This indicates that the 2D AgNPs/SiNSs nanocomposite is highly stable for catalytic applications.

3.3. Purification of 4-NP polluted water

To purify the water containing 4-NP pollutants, an experimental device of “filtering and catalyzing” was set up according to the literature [13], as shown in Fig. S3a. 50 mL of water containing 4-NP (0.12 mM) and NaBH_4 (12 mM) in a beaker was stirred at 800 rpm, and then 5 mL of AgNPs/SiNSs suspension (2 g/L) was rapidly added into the beaker. Several seconds later, the mixture was quickly filtered using a decompress filter. As a result, only 5 s later (Fig. S3b), the purified water exhibited a very light yellow, different from the bright yellow of raw 4-NP contaminated water (inset of Fig. S3a). Furthermore, after 10 s (Fig. S3c), the water was colorless, and the UV-vis absorption peak ascribed to 4-NP at around 400 nm was absent. It indicates the easy-using of 2D AgNPs/SiNSs nanocomposite for the highly efficient reduction of 4-NP.

4. Conclusions

In summary, the efficient assembly and high-density dispersion of uniform AgNPs with a narrow size distribution ranging from 1.6 to 4 nm (mean size = 2.77 nm) was achieved on the surface of 2D-SiNSs via a modified in-situ reduction approach. Further investigation found that AgNCs (< 2 nm) were first synthesised on the surface of 2D-SiNSs during the in-situ reduction reaction and subsequently grow into small

AgNPs during the washing process due to the absence of ammonia solution. Compared to the common reduction method using NaBH_4 , the loaded AgNPs on AgNPs/SiNSs nanocomposite have higher purity and the remaining Sn(II) species in AgNPs/SiNSs composite can effectively guarantee the stability of AgNPs. The catalytic reduction of 4-NP over the AgNPs/SiNSs nanocatalyst was almost completed within 40 s in the presence of NaBH_4 without stirring treatment. The apparent kinetic rate constant k_{app} ($80.19 \times 10^{-3} \text{ s}^{-1}$) is much higher than those of other substrate-supported Ag/Au nanocatalysts. The high-density dispersion of uniform small-sized AgNPs is responsible for the excellent catalytic performance of AgNPs/SiNSs nanocatalyst, which offers many active sites for effective contact with the reactants and fast interfacial electron transfer from the AgNPs surface to 4-NP. The results indicate a great potential of 2D silica nanosheets (derived from natural kaolinite mineral) as support materials for the efficient assembly of uniform noble-metal nanoparticles. Moreover, the 2D AgNPs/SiNSs nanocomposite is stable and easy to use for the highly efficient catalytic applications.

Acknowledgements

This work was supported by the National Natural Science Foundation of China (41572036), the Strategic Priority Research Program of Central South University (ZLXD2017005), the National Science Fund for distinguished Young Scholars (51225403), the National “Ten Thousand Talents Program” in China, the Hunan Provincial Science and Technology Project (2016RS2004, 2015TP1006) and the State Key Lab of Powder Metallurgy, Central South University (2015-19).

Appendix A. Supplementary data

Supplementary data associated with this article can be found, in the online version, at <https://doi.org/10.1016/j.apcatb.2017.12.040>.

References

- [1] R. Jin, Y. Charles Cao, E. Hao, G.S. Metraux, G.C. Schatz, C.A. Mirkin, *Nature* 425 (2003) 487–490.
- [2] S. Eustis, M.A. El-Sayed, *Chem. Soc. Rev.* 35 (2006) 209–217.
- [3] H.A. Atwater, A. Polman, *Nature Mater.* 9 (2010) 205–213.
- [4] R.R. Arvizu, S. Bhattacharyya, R.A. Kudgus, K. Giri, R. Bhattacharya, P. Mukherjee, *Chem. Soc. Rev.* 41 (2012) 2943–2970.
- [5] Z. Zhang, Y. Huang, K. Liu, L. Guo, Q. Yuan, B. Dong, *Adv. Mater.* 27 (2015) 5906–5914.
- [6] Y. Ma, X. Wu, G. Zhang, *Appl. Catal. B* 205 (2017) 262–270.
- [7] A. Desiréddy, B.E. Conn, J. Guo, B. Yoon, R.N. Barnett, B.M. Monahan, K. Kirschbaum, W.P. Griffith, R.L. Whetten, U. Landman, T.P. Bigioni, *Nature* 501 (2013) 399–402.
- [8] G. Liao, J. Chen, W. Zeng, C. Yu, C. Yi, Z. Xu, *J. Phys. Chem. C* 120 (2016) 25935–25944.
- [9] G. Liao, Y. Gong, C. Yi, Z. Xu, *Chin. J. Chem.* 35 (2017) 1157–1164.
- [10] G. Liao, W. Zhao, Q. Li, Q. Pang, Z. Xu, *Chem. Lett.* 46 (2017) 1631–1634.
- [11] G. Liao, Q. Li, W. Zhao, Q. Pang, H. Gao, Z. Xu, *Appl. Catal. A* 549 (2018) 102–111.
- [12] D. Astruc, F. Lu, J.R. Aranzaes, *Angew. Chem. Int. Ed.* 44 (2005) 7852–7872.
- [13] W. Ye, J. Yu, Y. Zhou, D. Gao, D. Wang, C. Wang, D. Xue, *Appl. Catal. B* 181 (2016) 371–378.
- [14] L.-S. Zhong, J.-S. Hu, Z.-M. Cui, L.-J. Wan, W.-G. Song, *Chem. Mater.* 19 (2007) 4557–4562.
- [15] Z. Zhang, C. Shao, P. Zou, P. Zhang, M. Zhang, J. Mu, Z. Guo, X. Li, C. Wang, Y. Liu, *Chem. Commun.* 47 (2011) 3906–3908.
- [16] Z. Zhang, C. Shao, Y. Sun, J. Mu, M. Zhang, P. Zhang, Z. Guo, P. Liang, C. Wang, Y. Liu, *J. Mater. Chem. B* 22 (2012) 1387–1395.
- [17] G. Eichenbaum, M. Johnson, D. Kirkland, P. O'Neill, S. Stellar, J. Bielawne, R. DeWire, D. Areia, S. Bryant, S. Weiner, D. Desai-Krieger, P. Guzzie-Peck, D.C. Evans, A. Tonelli, *Regul. Toxicol. Pharmacol.* 55 (2009) 33–42.
- [18] J. Li, Q. Liu, Q. Ji, B. Lai, *Appl. Catal. B* 200 (2017) 633–646.
- [19] C.V. Rode, M.J. Vaidya, R.V. Chaudhari, *Org. Process Res. Dev.* 3 (1999) 465–470.
- [20] Y. Du, H. Chen, R. Chen, N. Xu, *Appl. Catal. A* 277 (2004) 259–264.
- [21] S. Tang, S. Vonagehr, X. Meng, *J. Phys. Chem. C* 114 (2010) 977–982.
- [22] H.-L. Jiang, T. Akita, T. Ishida, M. Haruta, Q. Xu, *J. Am. Chem. Soc.* 133 (2011) 1304–1306.
- [23] S. Gao, Z. Zhang, K. Liu, B. Dong, *Appl. Catal. B* 188 (2016) 245–252.
- [24] Y. Fu, T. Huang, B. Jia, J. Zhu, X. Wang, *Appl. Catal. B* 202 (2017) 430–437.
- [25] K. Peng, L. Fu, J. Ouyang, H. Yang, *Adv. Funct. Mater.* 26 (2016) 2666–2675.
- [26] L. Fu, H. Yang, *Nanoscale Res. Lett.* 12 (2017) 411.

- [27] L. Fu, H. Yang, Y. Hu, D. Wu, A. Navrotsky, *Chem. Mater.* 29 (2017) 1338–1349.
- [28] L. Fu, H. Yang, A. Tang, Y. Hu, *Nano Res.* 10 (2017) 2782–2799.
- [29] K. Hou, J. Ouyang, C. Zheng, J. Zhang, H. Yang, *Mater. Express* 7 (2017) 104–112.
- [30] M. Long, Y. Zhang, Z. Shu, A. Tang, J. Ouyang, H. Yang, *Chem. Commun.* 53 (2017) 6255–6258.
- [31] K. Peng, L. Fu, H. Yang, J. Ouyang, A. Tang, *Nano Res.* 10 (2017) 570–583.
- [32] K. Peng, L.J. Fu, X.Y. Li, J. Ouyang, H.M. Yang, *Appl. Clay Sci.* 138 (2017) 100–106.
- [33] Z. Shu, Y. Zhang, Q. Yang, H. Yang, *Nanoscale Res. Lett.* 12 (2017) 135.
- [34] Y. Zhang, M. Long, P. Huang, H. Yang, S. Chang, Y. Hu, A. Tang, L. Mao, *Nano Res.* 10 (2017) 2633–2643.
- [35] Z. Yan, H. Yang, J. Ouyang, A. Tang, *Chem. Eng. J.* 316 (2017) 1035–1046.
- [36] S. Liu, Z. Yan, L. Fu, H. Yang, *Sol. Energy Mater. Sol. Cells* 167 (2017) 140–149.
- [37] Z. Yan, L. Fu, Y. Hu, H. Yang, *Adv. Mater. Interfaces* (2017), <http://dx.doi.org/10.1002/admi.201700934> in press.
- [38] K. Okada, A. Shimai, T. Takei, S. Hayashi, A. Yasumori, K.J.D. MacKenzie, *Micropor. Mesopor. Mater.* 21 (1998) 289–296.
- [39] M. Kerker, *The Scattering of Light and Other Electromagnetic Radiation*, Academic Press New York, 1969.
- [40] H.C. van de Hulst, *Light Scattering by Small Particles*, Wiley New York, 1957.
- [41] X. Wei, C. Shao, X. Li, N. Lu, K. Wang, Z. Zhang, Y. Liu, *Nanoscale* 8 (2016) 11034–11043.
- [42] Z. Zhang, J. Huang, Y. Fang, M. Zhang, K. Liu, B. Dong, *Adv. Mater.* 29 (2017) 1606688.
- [43] D.L. Van Hyning, W.G. Klemperer, C.F. Zukoski, *Langmuir* 17 (2001) 3120–3127.
- [44] B. Baruah, G.J. Gabriel, M.J. Akbashev, M.E. Booher, *Langmuir* 29 (2013) 4225–4234.
- [45] J. Zeng, Q. Zhang, J. Chen, Y. Xia, *Nano Lett.* 10 (2010) 30–35.
- [46] N.R. Jana, T. Pal, *Langmuir* 15 (1999) 3458–3463.
- [47] H. Zhang, X. Li, G. Chen, *J. Mater. Chem.* 19 (2009) 8223–8231.
- [48] J. Li, C. Liu, Y. Liu, *J. Mater. Chem.* 22 (2012) 8426–8430.
- [49] P. Zhang, C. Shao, Z. Zhang, M. Zhang, J. Mu, Z. Guo, Y. Liu, *Nanoscale* 3 (2011) 3357–3363.